TET2 suppresses vascular calcification by forming inhibitory complex with HDAC1/2 and SNIP1 independent of demethylation

Dayu He1, Jianshuai Ma1, Ziting Zhou1, Yanli Qi 1,2, Yaxin Lian1, Feng Wang1, Huiyong Yin 3*,Huanji Zhang1*,Tingting Zhang1*,and Hui Huang1*

1．Department of Cardiology, Joint Laboratory of Guangdong-Hong Kong-Macao Universities for Nutritional Metabolism and Precise Prevention and Control of Major Chronic Diseases, the Eighth Affiliated Hospital of Sun Yat-sen University, Shenzhen, 518033, China.

2．The Sixth Hospital of Wuhan，Affiliated Hospital of Jianghan University，Wu han, 430015, China.

3．Department of Biomedical Sciences, Tung Biomedical Science Center, The Shenzhen Research Institute and Futian Research Institute, College of Biomedicine, City University of Hong Kong, Hong Kong SAR, China.

Address correspondence to:

Hui Huang, Department of Cardiology, the Eighth Affiliated Hospital of Sun Yat-sen University, Shennan Middle Road, Shenzhen 510275, China. Phone: 86.755.83398398. Email: huangh8@mail.sysu.edu.cn.

Tingting Zhang, Department of Cardiology, the Eighth Affiliated Hospital of Sun Yat-sen University, Shennan Middle Road, Shenzhen 510275, China. Email: zhangtt73@mail.sysu.edu.cn.

Huanji Zhang, Department of Cardiology, the Eighth Affiliated Hospital of Sun Yat-sen University, Shennan Middle Road, Shenzhen 510275, China. Email: zhangtt73@mail.sysu.edu.cn.

Huiyong Yin, Department of Biomedical Sciences, Tung Biomedical Science Center, The Shenzhen Research Institute and Futian Research Institute, College of Biomedicine, City University of Hong Kong, Hong Kong SAR, China. Email: hyyin@sibs.ac.cn.

Authorship notes: Dayu He, Jianshuai Ma, and Ziting Zhou are co–first authors.

Conflict of interest: The authors have declared that no conflict of interest exists.

Abstract:

Osteogenic transdifferentiation of vascular smooth muscle cells (VSMCs) has been recognized as the principal mechanism underlying vascular calcification (VC). Runt-related transcription factor 2 (RUNX2) in VSMCs plays a pivotal role because it constitutes an essential osteogenic transcription factor for bone formation. As a key DNA demethylation enzyme, ten-eleven translocation 2 (TET2) is crucial in maintaining the VSMC phenotype. However, whether TET2 involves in VC progression remains elusive. Here we identified a substantial downregulation of TET2 in calcified human and mouse arteries, as well as human primary VSMCs. In vitro gain- and loss-of function experiments demonstrated TET2 regulated VC. Subsequently, in vivo knockdown of TET2 significantly exacerbated VC in both vitamin D3 and adenine-diet-induced chronic kidney disease (CKD) mice models. Mechanistically, TET2 binds to and suppresses the activity of the P2 promoter within the *RUNX2* gene, whereas an enzymatic loss-of-function mutation of TET2 has a comparable effect. Furthermore, TET2 forms a complex with histone deacetylases 1/2 (HDAC1/2) to deacetylate H3K27ac on the P2 promoter, thereby inhibiting its transcription. Moreover, SNIP1 is indispensable for TET2 to interact with HDAC1/2 to exert inhibitory effect on VC, and knockdown of SNIP1 accelerated VC in mice. Collectively, our findings imply that TET2 might serve as a potential therapeutic target for VC.

Key words: TET2, Vascular calcification, SNIP1, Demethylation, Smooth muscle cell

Graphical abstract

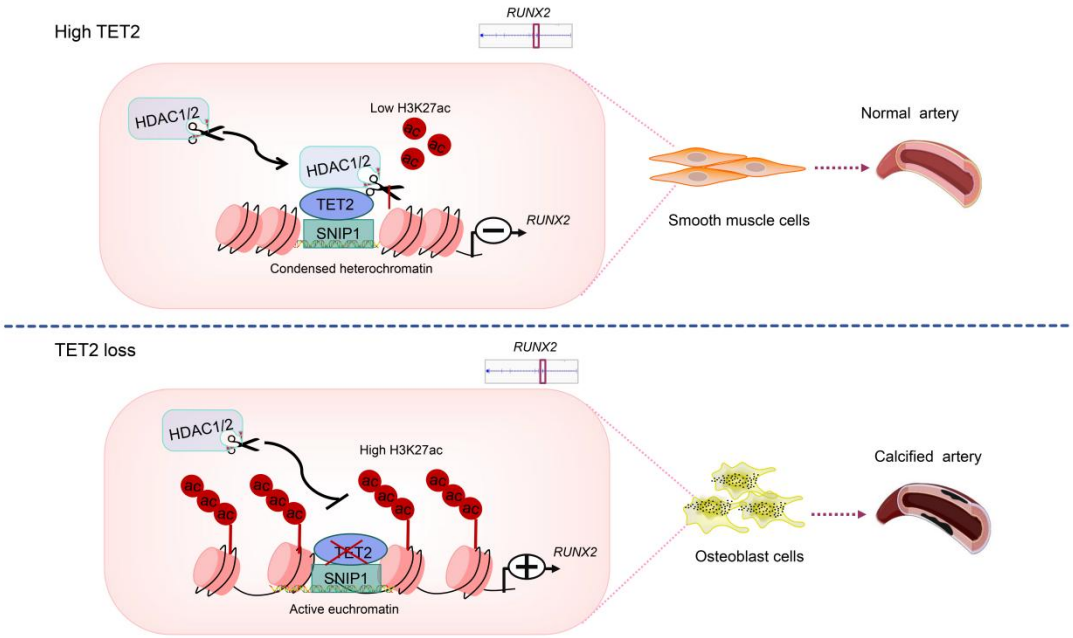

Introduction

Vascular calcification (VC), which constitutes a severe complication of chronic kidney disease (1) as well as diabetes mellitus (2), plays a significant role in contributing to high cardiovascular morbidity and mortality (3, 4). Among the various underlying pathogenesis that have been established in recent years, vascular smooth muscle cells (VSMCs) osteogenic transdifferentiation bears the key responsibility (5-8). Unlike most mature cells, VSMCs possess the ability to undergo plastic changes in response to environmental stimuli. VSMCs osteogenic transdifferentiation is one such pattern, characterized by the downregulation of VSMCs markers and the concurrent upregulation of osteogenic genes (9-11). The plasticity of VSMCs renders gene regulation a rather complex process. Several transcription factors have been identified, and among them, the runt-related transcription factor 2 (RUNX2) have been demonstrated to be a necessary and sufficient regulator for VSMC osteogenic differentiation(12, 13). Previous studies have disclosed a causal role of the RUNX2 in promoting the osteogenic transdifferentiation of VSMC (14-16). Moreover, it has been observed that RUNX2 expression remains low in healthy vascular but is remarkably increased in calcified arteries of animal models and in humans with CKD, atherosclerosis, and diabetes mellitus (17-20). Furthermore, specific deletion of RUNX2 in VSMCs within mouse models has indicated that loss of RUNX2 can inhibit vascular calcification (19, 21). It is worth noting that RUNX2 deletion did not lead to any alterations in the VSMCs phenotype or the normal development of the vascular (19, 21). However, a synergetic mechanism that collaboratively governs the VSMCs contractile phenotype and osteogenic transdifferentiation has yet to be

uncovered.

The ten-eleven translocation (TET) family of proteins, including TET1, TET2, and TET3 in mammalian cells, oxidize 5-methylcytosine (5-mC) to generate 5-hydroxymethylcytosine (5-hmC) (22). Pathologically, TET2 exhibits a close association with a spectrum of cardiovascular diseases (23, 24). Specifically, patients harboring a TET2 mutation or experiencing a loss of TET2 functionality are predisposed to an elevated risk of developing various cardiovascular pathology such as atherosclerosis (25), pulmonary hypertension(23), aortic valve stenosis, heart failure (26, 27). It is noteworthy that the majority of these diseases are often concomitant with a high incidence of vascular calcification (VC), highlighting the potential interplay between TET2 disorder and the manifestation of VC. Furthermore, studies revealed that TET2 is a master epigenetic regulator of VSMCs differentiation, and loss of TET2 leading to VSMCs dedifferentiation (28). As is known, possess the capacity to undergo transdifferentiation into alternative cell phenotypes, such as macrophage, synthetic, or osteogenic phenotype (10). however, the role of TET2 in VSMCs osteogenic transdifferentiation and its specific mechanisms are remained unclear. In this study, we explored the role of TET2 in VC. We observed a marked downregulation of TET2 in calcified groups in both clinical settings and mouse models. Further gain- and loss-of-function experiments revealed the protective role of TET2 on VSMCs osteogenic transdifferentiation. Mechanistically, our investigations uncovered that TET2 plays a crucial and necessary role in the inhibition of *RUNX2* gene transcription. This is achieved by forming an inhibitory complex in conjunction with other regulatory factors. The formation of such a complex constitutes a

key regulatory mechanism that intervenes in the transcriptional process of the *RUNX2* gene, which is a well-documented driver of osteogenic transdifferentiation in VSMCs. Most importantly, we have successfully illustrated the existence of a epigenetic regulator that functions in a synergistic manner to regulate both contractile and osteogenic genes within VSMCs. This discovery enriches our understanding of the intricate gene regulatory network governing VSMCs phenotype and function. Above all, we demonstrated a key role of TET2 on VC, and suggesting that targeting the TET2-HDAC1/2-SNIP1 complex pathway may be a potential choice for the inhibition of VSMCs osteogenic differentiation.

Results

TET2 is negatively correlated with VC in both human and mice specimens.

To investigate the role of TET2 in VC, we downloaded publicly available data of high - throughput sequencing from the Gene Expression Omnibus (GEO) database (GSE159832 and GSE254077). Heatmaps were utilized to showcase the expressions of *Tet2* and osteogenic genes (*Spp1, IL6, IL1a, and Bmp1*), and VSMC phenotype genes (*Myh11, Tagln*) in the apolipoprotein E knockout mice (*ApoE*$^{-/-}$) (atherosclerotic calcificaiton) aorta and β-glycerophosphate (β-GP) treatment induced calcified mice aorta. As depicted in the heatmaps, compared with the normal controls, the expression of TET2 was significantly decreased in the *ApoE*$^{-/-}$ mice aorta with atherosclerotic calcification lesion (Figure 1A) and β-GP treatment induced calcified mice aorta (Figure 1B). This suggested a crucial role of TET2 in vascular

142 calcification (VC). Furthermore, human leucocyte *TET2* mRNA levels were
143 evaluated in patients with CKD with VC (n = 24), CKD without VC (n = 12).
144 The basic characteristics of patients are shown in
145 Table 1. As is shown in Figure 1C, compared with non-calcified groups, *TET2*
146 mRNA levels were significantly decreased in patients with VC (95%CI
147 (8.258,4.024), P < 0.001). *TET2* mRNA levels were negatively related to
148 calcific score (R^2 = 0.68, P < 0.001) (Figure 1D) and *RUNX2* mRNA levels (R^2
149 = 0.45, P < 0.001) (Figure 1E). Additionally, we also detect *TET2* mRNA
150 levels from healthy people (n=21), finding that, compared to the normal
151 people, *TET2* significantly decreased both in CKD patients with or without VC
152 (Supplemental Figure 1A and 1B). Then we detected TET2 levels in calcified
153 and non-calcified human arteries. The calcified arteries were collected from
154 patients with CKD undergoing arterial venous fistula operation and diagnosed
155 with aortic arch calcification (CKD, n = 6). Additionally, the control arteries
156 were obtained from patients who underwent amputation surgery due to upper
157 limb trauma, without a diagnosis of CKD or diabetes mellitus (control, n = 6).
158 Both immunofluorescence (IF) staining (Supplemental Figure1C) and
159 Immunohistochemical (IHC) staining (Figure 1F) revealed that TET2
160 expression was substantially decreased in calcified human arteries.
161 Furthermore, we tested TET2 levels in calcified aorta of mice injected with
162 vitamin D3. Both IHC results (Figure 1G) and western blot analysis (Figure 1H)
163 confirmed a marked downregulation of TET2 in the calcified mouse aorta.
164 Then we detected TET2 expressions in high inorganic phosphate (Pi)-induce
165 human primary aorta vascular smooth muscle cells (hVSMCs) calcification
166 and discovered that TET2 significantly declined as Pi-induced time increased

(Figure 1I).

TET2 plays a role in human primary VSMCs osteogenic transdifferentiation.

To assess the causal role of TET2 in hVSMCs osteogenic reprogramming, we constructed lentivirus carrying short hairpin RNA (shRNA) specific to the human *TET2* gene (*shTET2*) (Supplemental Table 6). As western blot data shown, the TET2 was substantially knocked down in hVSMCs (Supplemental Figure 3A). Results indicated that depletion of TET2 significantly exacerbated hVSMCs calcification, which was ascertained through Alizarin Red S staining (Figure 2A), the quantification of ALP activity (Figure 2C), and the calcium assay (Figure 2D). Additionally, further Western blot analysis disclosed a substantial upregulation in the expression of osteogenic differentiation genes, including OPN and RUNX2, while there was a marked downregulation of VSMCs phenotype genes, including smoothelin and SM22α (Figure 3G). Conversely, the overexpression of TET2 via adenovirus markedly mitigated the Pi-induced hVSMCs calcification. This was gauged by Alizarin Red S staining (Figure 2B), the quantification of ALP activity (Figure 2E), and the calcium assay (Figure 2F). The Western blot analysis showed a significant downregulation in the expression of osteogenic differentiation genes, including OPN and RUNX2, while there was a marked upregulation of VSMC phenotype genes, including smoothelin and SM22α (Figure 3H). Taken together, these results suggest that TET2 serves to inhibit the osteogenic transdifferentiation of hVSMCs.

VSMCs specific loss of Tet2 in mice aggravated vascular calcification.

In order to investigate the potential role of Tet2 in vivo, we employed adenoassociated virus 9 (AAV9) with transgelin (TAGLN) promoter to achieve VSMC-specific knockdown of Tet2 in mice. AAV with scrambled shRNA *(AAV-sh-Scr*) or *Tet2* shRNA (*AAV-sh-Tet2*) were presented in supplemental Table 7. The knockdown efficiency of Tet2 in the aorta was evaluated by Western blot analysis (Supplemental figure 3B). We constructed both vitamin D3 model and adenine-diet-induced CKD model to investigate the role of Tet2 in in vivo calcification. We tested several key systemic parameters, including those related to liver function such as Alanine Transaminase (ALT) and Aspartate Transaminase (AST), as well as those associated with renal function like serum urea nitrogen and creatinine. Additionally, we also examined systemic metabolism parameters such as calcium levels, and body weight. Our findings revealed that there were no significant difference in these aspects between the *AAV-sh-Scr* groups and the *AAV-sh-Tet2* groups (Supplemental Table 2 and 3). However, it was notable that the level of serum alkaline phosphatase (ALP) was significantly elevated in the *AAV-sh-Tet2* groups (Supplemental Table 2 and 3). As depicted in Figure 3A and Figure 3E, the loss of Tet2 significantly aggravated the calcium deposition and mineralization in the aorta compared to the *sh-Scr* controls, as confirmed by Alizarin Red S staining. Consistently, Von Kossa staining demonstrated substantially increased calcium deposition in the aortic sections of Tet2 knockdown mice (Figure 3B

and Figure 3F). IHC staining indicated a substantially higher Runx2 expression in the *AAV-sh-Tet2* groups than in the *AAV-sh-Scr* groups (Figure 3C). Moreover, Western blot and quantification analysis revealed that, in contrast to the *AAV-sh-Scr* groups, the *AAV-sh-Tet2* groups exhibited significantly higher osteogenic markers Runx2 and Opn, while the VSMC contractile markers Smoothelin and SM22α were lower (Figure 3D and Figure 3G). Collectively, we validated the effects of Tet2 on calcification using two distinct calcified models.

TET2 inhibits *RUNX2* gene transcription not by DNA demethylation but by decreasing H3K27ac on the P2 promoter.

To investigate the specific mechanisms underlying the role of TET2 in VC, and given the crucial role of RUNX2 in VC, we initially carried out q-PCR experiments to analyze the mRNA levels of *RUNX2*. As is depicted in Figure 4A and 4B, the mRNA level of *RUNX2* was significantly upregulated in the TET2 knockdown groups (Figure 4A), while substantially inhibited in the TET2 overexpressed groups (Figure 4B). To examine whether TET2 regulates *RUNX2* gene transcription, we analyzed the TET2-enriched chromatin based on the data from chromatin immunoprecipitation sequencing (ChIP-seq). It is known that *RUNX2* gene transcription is governed by two promoters, namely the distal P1 promoter and the proximal P2 promoter, which encode two major isoforms via exons 1–8 (type II) or exons 2–8 (type I) (supplemental Figure 2)

(29, 30). The results of CHIP-seq demonstrated that TET2 peaks were distributed across the *RUNX2* genome, with a substantially higher enrichment on the P2 promoter compared to the P1 promoter (Figure 4C) (31). Considering that TET2 is recognized to contribute to DNA demethylation (22, 28), we tested 5-methylcytosine (5 mc) levels in the *RUNX2* P2 promoter using MethylCap coupled with qPCR. Surprisingly, in contrast to the control groups, 5 mc levels remained unchanged, neither in the TET2 knockdown groups nor in the TET2 overexpressed groups (Figure 4E and 4D).

To investigate whether the binding of TET2 modulates *RUNX2* gene transcription, a luciferase reporter driven by the *RUNX2* promoter was carried out using either the P1 or P2 promoter. Our results demonstrated that overexpression of TET2 significantly suppressed the luciferase activity of the P2 promoter (Figure 4G), while having no effect on that of the P1 promoter (Figure 4F). In contrast to the wild-type TET2, an enzymatically inactive mutant form of TET2 exhibited a comparable inhibitory effect on the luciferase activity of the P2 promoter (Figure 4G). Moreover, Data from Assays for Transposase-Accessible Chromatin with high-throughput sequencing (ATAC-seq) were analyzed to investigate the chromatin accessibility of the *RUNX2* gene under different *TET2* interventions. We observed that, compared to the *TET2*-wild type (*TET2*-WT) group, *TET2*-knockout (*TET2*-KO) resulted in a greater chromatin accessibility, as manifested by an marked increased level of annotated peak in the *RUNX2* P2 promoter (Figure 4H). This indicates that

TET2 knockout led to the inhibition of P2 promoter (GSE241347). However, ATAC-seq revealed no significant difference between the *TET2-WT* and the *TET2* loss-of-function mutations (*TET2-MUT*) groups (Figure 4I) (32), suggesting that the inhibitory role of TET2 at the P2 promoter is independent of its enzymatic function.

In order to examine the function of TET2 binding to the *RUNX2* promoter in the context of vascular calcification, we carried out CUT&Tag coupled with qPCR (CUT&Tag-qPCR). An anti-TET2 antibody was used to immunoprecipitate protein-DNA complexes from both control and Pi-induced VSMC. Subsequently, the *RUNX2* P1 (CUT1) and P2 (CUT2) promoters were amplified via qPCR (Figure 4J). The results indicated that TET2 was predominantly enriched on the P2 promoter and to a lesser extent on the P1 promoter. Notably, the enrichment on the P2 promoter was significantly reduced during osteogenic transdifferentiation of hVSMCs induced by Pi (Figure 4J). Beyond their established roles in DNA oxidation, tet proteins have been reported to functionally interact with other epigenetic modifiers, thereby inducing chromatin remodeling and consequent gene transcription (33-35). In light of these findings, we performed CUT&Tag-qPCR by immunoprecipitating with antibodies that recognize the active mark of promoters, specifically the acetylation of lysine 27 on histone 3 (H3K27ac). As expected, we detected an substantially elevated enrichment of H3K27ac at the *RUNX2* P2 promoter compared to the P1 promoter following Pi-induced hVSMCs osteogenic

transdifferentiation (Figure 4K), signifying the establishment of an open chromatin conformation at the *RUNX2* P2 promoter. Compared to the control vector, knockdown of TET2 led to a significantly increase in the H3K27ac levels at the P2 promoter in hVSMCs (Figure 4L). Conversely, overexpression of TET2 markedly reduced the H3K27ac levels at the P2 promoter, indicative of a repressive chromatin state (Figure 4M).

Collectively, all of the aforementioned results validated that TET2 directly suppresses *RUNX2* gene transcription by diminishing its H3K27ac levels on the P2 promoter, rather than through its DNA demethylation function.

TET2 interact with HDAC1/2 to suppress the activity of *RUNX2* P2 promoter through deacetylating H3K27ac.

Previous evidence suggested that two histone deacetylases, HDAC1/2, were associated with a majority of genes marked with H3K27ac and coexisted in several polyprotein repressive complexes that silenced genes (36). This suggested their potential roles in regulating VSMCs osteogenic transdifferentiation in conjunction with TET2. Firstly, we verified the endogenous interactions between TET2 and HDAC1/2 in hVSMCs (Figure 5A). Subsequently, a luciferase reporter assay driven by the *RUNX2* promoter was carried out using the P2 promoter. We discovered that knockdown of HDAC1/2 significantly reversed the inhibitory effect of TET2 on the luciferase activity of the *RUNX2* P2 promoter. Similar reversed outcomes were also

observed in the case of the enzymatically mutated form of TET2 (Figure 5B).

To explore whether HDAC1/2 were involved in the regulation exerted by TET2 on *RUNX2*, we performed CUT&Tag-qPCR by immunoprecipitating H3K27ac in hVSMC overexpressing TET2 and simultaneously transfected with *si-Scr*, *si-HDAC1, si-HDAC2*, *or si-HDAC1/2* separately. The results demonstrated that the H3K27ac marks increased slightly in the *si-HDAC2* group but showed no difference in the *si-HDAC1* groups, while significantly rising in the *si-HDAC1/2* group (Figure 5C). To further investigate the recruitment of HDAC1/2 to the *RUNX2* P2 promoter by TET2, we conducted CUT&Tag-qPCR using HDAC1 and HDAC2 antibodies separately. The results revealed that the binding of both HDAC1 (Figure 5D) and HDAC2 (Figure 5G) was dramatically decreased at the *RUNX2* P2 promoter after Pi stimulation. The enrichment of HDAC1 (Figure 5E) and HDAC2 (Figure 5I) at the P2 promoter declined in the TET2 knockdown groups, while substantially increased after TET2 overexpression (Figure 5F and 5H). Given that HDAC1 might compensate for the absence of HDAC2 at the *RUNX2* P2 promoter, we detected HDAC2 binding after the knocking down HDAC1 and confirmed a marked reduction of HDAC2 at the P2 promoter (Figure 5J). These results imply that TET2 and HDAC1/2 form an inhibitory complex to inhibit the P2 promoter and consequently repress *RUNX2* gene transcription. In this complex, HDAC2 may serve as the key enzyme for deacetylating H3K27ac, while HDAC1 might act as a compensatory factor in the event of HDAC2 loss.

TET2 inhibits VC by interacting with HDAC1/2.

Subsequently, we delved into whether HDAC1/2 participated in the regulatory mechanism of TET2 in suppressing VC. By simultaneously knocking down HDAC1/2 and overexpressing TET2, we discovered that the knockdown of HDAC1/2 remarkably offset the protective effect of TET2 against hVSMCs calcification. This was evidenced by Alizarin Red S staining (Figure 6A), quantification of ALP activity (Figure 6B) and calcium assay (Figure 6C). Moreover, further Western blot analysis demonstrated that, in contrast to the group with TET2 overexpression and si-Scr intervention, the group with TET2 overexpression and *si-HDAC1/2* intervention exhibited a substantially greater expression of osteogenic differentiation genes, including OPN and RUNX2, while presenting a lower expression of VSMCs phenotype genes, including Smoothelin and SM22α (Figure 6D and 6E). Notably, the knockdown of HDAC1/2 was both highly efficient and specific (Supplemental Figure 3E and 3D).

SNIP1 is necessary for TET2 to interact with HDAC1/2 at the *RUNX2* P2 promoter.

TET2 lacks a CXXC DNA binding domain and is likely to bind to specific genes through other proteins, like cell-type-specific transcription factors (37-40). Previous findings have identified SMAD nuclear interacting protein 1 (SNIP1) as one of the potential interacting transcription regulators that interact with TET2 (41, 42). SNIP1 is recognized as a transcription repressor which inhibits the BMP signaling pathway by directly interacting with its intracellular

effectors, the SMAD2/3 proteins, thereby limiting its functions (43). There is evidence suggesting that SNIP1 inhibits the TGF- /BMP-signaling pathways by interfering with the interaction of SMAD2/3 and the histone acetyltransferase CBP/p300 (41). As is commonly known, the BMP signaling pathway is a key pathway in osteogenic differentiation, and its intracellular effectors, the SMAD2/3 proteins, are the key transcription factors for the transcriptional activation of *RUNX2* gene (6, 44-46). Taking the above evidence into account, we investigated whether SNIP1 is involved in the transcriptional inhibition exerted by the TET2-HDAC1/2 complex at the P2 promoter of *RUNX2* gene. Firstly, we analyzed the CHIP-seq data (47) regarding on chromatin enriched with SNIP1 and detected a significant peak of SNIP1 at the *RUNX2* P2 promoter (Figure 7A). Subsequently, we analyzed the binding motif within the ChIP-seq peaks where TET2 and SNIP1 co-bind, and found the presence of SMAD2 motifs in the co-occupied peaks (Figure 7B). Furthermore, we identified the endogenous interactions between SNIP1 and TET2, and also found that SNIP1 interacted with HDAC1/2 in hVSMCs (Figure 7C). We hypothesized that SNIP1 might enhance the interaction between TET2 with HDAC1/2. Hence, we carried out CO-IP experiments under the condition of SNIP1 knockdown. It was observed that, compared to the control groups, the absence of SNIP1 led to a substantially reduced interaction between TET2 and HDAC1/2 (Figure 7D). Then, a luciferase reporter assay driven by *RUNX2* promoter, specifically using the P2 promoter. We noticed that the knockdown of SNIP1 significantly reversed the repressive effect of TET2 on the luciferase activity of P2 promoter (Figure 7E), and similar reversed outcomes were seen in the enzymatic mutation form of TET2

(Figure 7E). To further investigate the in vivo interaction of SNIP1 and TET2 on the P2 promoter, we performed CUT&Tag-qPCR. We found that after SNIP1 knockdown, the binding of TET2 at the P2 promoter significantly decreased (Figure 7F). Similarly, the enrichment of HDAC1/2 also substantially declined (Figure 7G and 7H), while H3K27ac was markedly increased (Figure 7I). Western blot data showed that the knockdown of SNIP1 was highly efficient (Supplemental Figure 3C). In conclusion, all these findings lead us to the conclusion that SNIP1 is essential for TET2 to interact with HDAC1/2 at the *RUNX2* P2 promoter and consequently for the removal of H3K27ac.

SNIP1 is vital for TET2 to impede hVSMCs osteogenic transdifferentiation.

We proceeded to investigate the role of SNIP1 in VC. As anticipated, the overexpression of SNIP1 in hVSMCs significantly alleviated VC and reduced RUNX2 expression (Supplemental Figure 4A and 4B). To ascertain whether SNIP1 mediates the osteogenic reprogramming of VSMCs regulated by TET2, hVSMCs were transfected with *Lenti-sh-SNIP1* in combination with *Ad-TET2*. We observed that the loss of SNIP1 significantly attenuated the inhibitory effect of TET2 on hVSMCs calcification and RUNX2 expression (Figure 8A and 8C). Subsequently, hVSMCs were transfected with *Lenti-sh-TET2* along with *Ad-SNIP1*. Results confirmed that the knockdown of TET2, in the context of SNIP1 overexpression, largely reversed the protective effects of

SNIP1 on hVSMCs calcification and RUNX2 expression (Figure 8B and 8D). These findings, therefore, conclusively demonstrate that SNIP1 is essential for TET2 to inhibit VC.

Knockdown of Snip1 accelerated vascular calcification in mice.

To gain a more comprehensive understanding the role of SNIP1 on VC, we employed the adeno-associated virus (AAV) infection as a genomic manipulation model. AAVs with *TAGLN* promoter carrying either scrambled shRNA or *Snip1* shRNA (*sh-Snip1*) were administered via the tail vein in vitamin D3-induced mouse models. The depletion of Snip1 in the aorta was verified through Western blot analysis (Figure 9A). The loss of Snip1 remarkably augmented the calcium deposition and mineralization in the aorta when compared to the scrambled controls, as confirmed by Alizarin Red S staining (Figure 9B). Consistently, Von Kossa staining demonstrated substantially increased calcium deposition in the aortic sections of Snip1 knockdown mice (Figure 9C). Further western blot analysis indicated a significantly increased expression of osteogenic genes Runx2, while a markedly decreased expression of VSMCs genes including Smoothelin and SM22α (Figure 9D). Taken together, these results indicate that a deficiency of Snip1 accelerates VC.

Discussion

In this work, we identified TET2 as a inhibitor of VSMCs osteogenic transdifferentiation, which functions directly to repress the transcription of *RUNX2* gene. Through a comprehensive series of in vitro and in vivo experiments, we have firmly established a crucial role of TET2 in inhibiting VSMC calcification. Notably, TET2 expression is downregulated in calcified samples from both humans and mice models. Experiments involving TET2 deletion and overexpression established a causal role between TET2 and VSMC calcification, such that TET2 deficiency exacerbates VC, whereas TET2 overexpression leads to a significantly attenuation of VC. In addition, application of human arteries with and without calcification from the same vascular sites will be better to bolster our findings.

Previous evidence has suggested a close correlation between TET2 and cardiovascular disease (24, 25, 48), as well as its significance in the normal differentiation of VSMCs (28). However, the effects of TET2 on VC still remains a mystery. In this study, we revealed the critical role of TET2 on VC and discovered that RUNX2 may be the target of TET2 protecting VSMCs from VC. As we have known, VSMCs have plastic ability and are able to differentiate into other cell types in response to environmental changes (9, 49), and VSMCs osteogenic transdifferentiation is one of the results. Previous results show that TET2 is a master regulator of maintaining the VSMC contractile phenotype by altering DNA methylation to promote the expression of *MYOCD*, *SRF*, and other contractile genes (28). Also, they discovered a coordinate suppression of *KLF4* and other de-differentiation related genes in VSMCs (28), but what directs TET2 mediating the opposing effects on

444 contractile and dedifferentiated genes are still unclear. Now, we confirmed
445 that TET2 is essential and necessary to VSMCs osteogenic
446 transdifferenciation. We conclude that the absence of TET2 in VSMCs results
447 in the repression of VSMC contractile genes, but the activation of *RUNX2*
448 gene transcription. Ectopic expression of TET2 in VSMCs not only promote
449 the expression of VSMCs contractile genes but also contribute to the
450 repression of osteogenic genes. Taken together, these results may offer us
451 clues on why dedifferentiation of VSMCs possesses the ability to
452 transdifferentiate into osteogenic cells instead of other phenotypes, and the
453 loss of TET2 in VSMCs may be the key culprits.

454 Mechanistically, we found that TET2 can bind to the *RUNX2* gene P2
455 promoter and repress its activity, and the enzymatic loss-of-function mutation
456 had the same effect. Independent of its DNA demethylation function, we found
457 that TET2 facilitate HDAC1/2 bind to the *RUNX2* P2 promoter, which led to
458 histone deacetylation-mediated inhibition of *RUNX2*. Moreover, SNIP1 is
459 necessary for TET2 to interact with HDAC1/2 at the *RUNX2* P2 promoter and
460 is vital for TET2 to hinder VC. Furthermore, most regulators of *RUNX2*
461 transcription reported to date concentrate on its P1 promoter (the remote
462 promoter)(29, 50, 51). Here, we provide the evidence that TET2 correlates
463 with *RUNX2* transcription inhibition by binding to the special locus of its P2
464 promoter (the proximal promoter).

465 Compelling evidence of TET proteins today have concentrated on their
466 DNA demethylation function (22, 28, 48), but the functions of TET2 and the
467 effects of its enzymic loss mutations in vascular calcification are largely
468 unknown. In this study, we show that, independent of the DNA demethylation

roles, TET2 coordinated with HDAC1/2 to inhibit *RUNX2* gene transcription, and the enzymatic mutations had the same effects. Previous studies have revealed that, except for the known regulatory roles in DNA demethylation, TET proteins are able to coordinate with other epigenetic modifiers to induce multi-layer chromatin regulation. For example, it has been reported that TET2 can connect with H3K4 methylation to upregulate gene transcription (33, 35). TET1 has also been revealed to participate in the silencing of developmental genes in embryonic stem cells (52). Recently, the repressing roles of TET2 and its non-enzymatic function have begun to be understood. In line with our study, a study revealed that TET2 can repress gene transcription in chromatin not by its catalytic activity, but by interacting with the histone deacetylase complexes (36). Another observation also suggested that PSPC1 and TET2 can act together with histone deacetylase complexes for transcriptional silencing of MERVL and is independent of TET2 catalytic activity (53).Studies also show that interferon signaling was restrained by TET2 in human macrophages, and the DNA methylation lacks correlation with the activation of IFN signaling. They found that TET2 interacts with RBPJ and ZNF143 in regulatory regions of the transcription factor A mitochondria (*TFAM*) gene to regulate the expression of the *TFAM* gene (54). Moreover, our study is also consistent with other reports, which revealed that the loss of catalytic roles of TET2 are crucial to the homeostasis in hematopoietic stem and progenitor cell (55).

Increasing evidence has revealed that most chromatin-modifying enzymes are not bind to the target DNA by themselves (56), but are recruited to the specific genes by other factors to regulate their expression and the

cellular processes. In this study, we discovered the critical role of TET2 on the *RUNX2* gene transcription. TET2, however, is unable to bind to target genes by themselves (37, 38), and previous studies have reported the co-regulating roles of SNIP1 in TET2 regulation (42). Given the inhibitory functions of SNIP1 in the BMP2 signaling pathway (41), which is a major pathway of osteogenic differentiation, and its intracellular effectors SMAD2/3 proteins play key roles in the activation of *RUNX2* gene transcription (44-46). We therefore investigated the roles of SNIP1 in *RUNX2* gene transcription and VSMCs osteogenic transdifferentiation. We discovered that SNIP1 can bind to the *RUNX2* P2 promoter, and we analyzed the binding motif in TET2 and SNIP1 co-bound ChIP-seq peaks, which revealed the presence of SMAD2 motifs in the co-occupied peaks. Further, we found that SNIP1 is necessary for TET2 to interact with HDAC1/2 at the *RUNX2* P2 promoter and is vital for TET2 to hinder VC. Our findings are concordant with previous work, which shows that SNIP1 is a transcription repressor in inhibits the BMP signaling pathway by interacting directly with SMAD2/3 proteins to limit its effects (43). Evidence also suggests that SNIP1 inhibits TGF- /BMP-signaling pathways by interfering with the interaction of SMAD2/3 with the histone acetyltransferase CBP/p300 (41).

Collectively, the current research endeavor has elucidated the pivotal role played by TET2 in safeguarding VSMCs against VC. It has furnished a novel and hitherto uncharted mechanism explicating how the deficiency of TET2 within VSMCs triggers their dedifferentiation process and subsequent transdifferentiation specifically into osteogenic cells, rather than alternative cell phenotypes. Moreover, we have unearthed the function of the TET2-

519 HDAC1/2-SNIP1 complex in the transcriptional regulation of the *RUNX2* gene.
520 This finding imparts perspectives into the underlying biochemical mechanism
521 by which TET2 exerts its inhibitory effect on gene transcription, thereby
522 enhancing our comprehension of the molecular underpinnings governing
523 VSMC fate determination and the pathophysiological processes associated
524 with VC.
525

526 ## Methods

527 ### Sex as a biological variable

528 Sex was not considered as a biological variable in human samples and no
529 difference was found between sexes. Our study performed experiments on
530 male and female mice, with similar findings reported for both sexes.
531

532 ### Human samples

533 Human arteries were collected from patients with CKD undergoing arterial
534 venous fistula operation and diagnosed with aortic arch calcification (CKD, n =
535 6). Additionally, the control arteries were obtained from patients who
536 underwent amputation surgery due to upper limb trauma, without a diagnosis
537 of CKD or diabetes mellitus (control, n = 6). Blood samples were collected
538 from CKD patients with calcification (n = 24) and without calcification (n = 12),
539 and healthy people (n = 21). Histopaque-1077 (Sigma) gradient were used to
540 extract PBMCs from blood. We collected the clinical and biochemical
541 parameters of related participants from the electronic medical system in the
542 hospital. Relative clinical samples were collected from Donghua Hospital of
543 Sun Yat-sen University from November 2019 to January 2020.

Animal experiments

Our study performed experiments on male and female mice. 8-weeks-old C57BL/6J mice were purchased from the Laboratory Animal Center of Sun Yat-sen University. To build TET2 specific VSMCs knockdown mice, we first constructed recombinant adeno-associated virus (AAV) serotype 9 gene transfer vectors carrying transgelin (*TAGLN*) promoter and *sh-TET2* or *sh-Scr*, and injected into the lateral tail vein of mice. The *sh-TET2* sequence is listed in Supplemental Table 7. After 4 weeks, we sacrificed few mice with isoflurane (induction 5%, maintenance 2%) and collected the aortas to verify the efficiency of *AAV-sh-TET2* in aortas. Then, to induce arterial medial calcification we randomly injected with vitamin D3 (5.5 105 U/kg/day) 3 days in the mice as previous described (57). About 7 days later we the sacrificed the mice and collected the whole aortas for the following experiments. For the adenine diet–induced CKD model, mice were randomly provided with a chow diet as the control group, or a special diet containing 0.2% adenine, 1.2% phosphorus as the CKD group. Four weeks subsequent to the commencement of the specialized diet regime, the mice were administered with the specified virus (at a dosage of 5×10^9 plaque-forming units per kilogram of body weight per mouse) via the tail vein injection method. After a lapse of four weeks, the mice were subjected to overnight fasting. Their body weights were recorded prior to euthanasia, and blood samples were collected. Subsequently, the entire aortas were harvested and meticulously dissected for further in-depth analyses.

Alizarin red staining

Alizarin red staining was performed to determine hVSMCs and mice aortas calcification. Firstly, wash cells with PBS, then fixed with 4% para formaldehyde. Next, wash with distilled water. Finally, add 1% Alizarin red Solution and incubated for 15 minutes, then washed with distilled water. For mice aortas, 4% para formaldehyde fixed for 24 hours, and staining with 0.003% Alizarin red solution in 1% sodium hydroxide for 30 hours, and then washed with 1% sodium hydroxide. Positive results would present as a reddish color which means calcification.

Von Kossa staining

Slides of mice aorta were being deparaffinized and rehydrated, then incubated in 5% silver nitrate and following that expose to ultraviolet light about 1 hour until the color reaction down. Finally treated the slides with 5% sodium thiosulfate and washed twice with double distilled water. Calcified area would be stained as brown to black.

Calcium and ALP quantification

For calcium quantification, first wash the cells softly with PBS for 3 times, incubated the VSMCs with 0.6 mol/L HCl overnight at 4°C. Then collect the supernatant. Then use a commercial kit (Biosino Bio-Technology and Science) to measure the calcium content according to the manufacturer's instructions. For ALP quantification, incubate the VSMCs with 1% Triton X-100 in 0.9% saline on ice, then collect the supernatant and centrifugation in a microfuge at 8000*g* for 5 minutes. Secondly, using a commercial assay kit

(Biosino Bio-Technology and Science) to analyze the ALP activity. Results are normalized by the total protein levels.

Laboratory analyses

Mice blood levels of blood urea nitrogen (BUN), creatinine (CREA) were measured by autoanalyzer (Hitachi). Plasma levels of calcium were measured using the detection kit (Biosino Bio-Technology and Science). Plasma levels of ALP were measured using a commercial assay kit (Biosino Bio-Technology and Science). Plasma levels of alanine transaminase (ALT), aspartate aminotransferase (AST) were analyzed using ELISA kits (Jiangsu Meimian industrial), according to the manufacturer's instructions.

Co-immunoprecipitation

Incubated the VSMCs Lysis Buffer with corresponding antibody and IgG overnight at 4ºC. Place Pierce Protein A/G Magnetic Beads, then add Wash Buffer wash the beads twice. Add the antigen sample/antibody mixture and incubate at room temperature for 1 hour. Collect the beads and repeat wash twice. Then add purified water wash once. Finally add Low-pH Elution Buffer and incubate for 10 minutes. Add Neutralization Buffer to neutralize the low pH, then boiled with sodium dodecylsulfate buffer and analyzed by Western blot.

Reverse transcription and real-time polymerase chain reaction (PCR)

Total RNA was extracted from peripheral leukocytes or cultured cells by Trizol Reagent (Takara, Japan, 9109), and reverse-transcribed into cDNA with a

Prime ScriptRT Reagent Kit (Takara, RR036A). Real-time PCR was performed using Bio-Rad SYBR Green on a CFX96 Touch Real-Time PCR Detection System (Bio-Rad). GAPDH was used as a reference and was calculated according to the 2ΔΔCt method. Primers sequences are listed in Supplementary Table 5.

Immunohistochemical staining

The sections were heated at 60 °C for 1 h and deparaffinized and rehydrated. 0.3% H2O2 were used to block Endogenous peroxidase activity for 20 minutes. 10% citrate buffer and Heat for antigen retrieval. Then primary antibodies incubated overnight at 4°C followed by a EnVision+ Dual Link System-HRP for 1 h at room temperature. Finally, DAB peroxidase substrate kit (ZSGB bio, Cat#2L2-9018) were stained for 1 min. Images were captured with light microscopy (Nikon NiU).

Data analysis

Normalization of gene counts and identification of related genes were performed by using DESeq2. The software Enriched domain detector was used to detect wide genomic enriched domains. By enriched domain detector, we calculate the TET2, SNIP1, and ATAC-enriched signal compared with input. Bigwig files were generated by the $\log_2$ ratio fold-change against input, and using the Integrative Genomics Viewer to visualize them.

Statistics

GraphPad Prism 9.0 software were used to analyze all of the data. Values

were presented as mean ± SEM deviation. Student' s t test or nonparametric Mann-Whitney U test were performed to compare 2 groups. ANOVA analysis followed by the post hoc Bonferroni's or Dunnett's test were performed to compare the multiple groups. Pearson's correlation coefficient analysis was used to value the statistical correlations. Statistically significant was considered by Two-tailed $P < 0.01$ (indicated by **), $P < 0.05$ (indicated by *).

Study approval

The collection of related species from patients were approved by all donors enrolled in this study. This study was conducted in accordance with the Declaration of Helsinki and was approved by the internal review and ethics Committee of the Donghua Hospital of Sun Yat-sen University (SYSEC-KY-KS-2020-191). The experimental animal protocols were approved by the Ethics Committee of Shenzhen TopBiotech Co., Ltd (TOP-IACUC-2023-0198).

Data availability

Data for bulk RNA-seq analysis were from the database GSE159832 and GSE254077 in GEO (https://www.ncbi.nlm.nih.gov/geo/). TET2 and SNIP1 ChIP-seq raw data and ATAC-seq raw data were from the public GEO database as GSM7996293, GSE175848, GSE241347 and GSE213768 for analyses. The data supporting the findings of this study are included in the main article, supplemental materials, and Supporting Data Values file.

Author contributions

D. H. and H. H. designed the research. D. H. and J. M. performed most of the experiments. Z. Z., H. Z. performed the animal experiments and analyzed the data. Y. Q., Y. L. and F. W. performed some of the biochemical and biophysical experiments. D. H. and H. H. wrote the manuscript with comments from all authors. H. H.. T. Z. and H. Y. polished the manuscript. T. Z.,H. Z. and H. Y. supported the manuscript. All authors in this manuscript approved this final version. We determined the order of co-first authors by their efforts and contributions to this project.

Acknowledgments

This work was supported by Shenzhen Science and Technology Program (ZDSYS20220606100801004, KCXFZ20211020163801002, SGDX20230116092459009, JCYJ20220530144417039, JCYJ20230807110913027), Shenzhen Medical Research Fund (B2302020), National Natural Science Foundation of China (82330021, 82270771, 82204384, 82473913), and Shenzhen Key Medical Discipline Construction Fund (SZXK002), Futian District Public Health Scientific Research Project of Shenzhen (FTWS2022001, FTWS2022025), Chinese Association of Integrative Medicine-Shanghai Hutchison Pharmaceuticals Fund (HMPE202202), China Heart House-Chinese Cardiovascular Association HX fund (2022-CCA-HX-090), RGC General Research Fund (T12-101/23-N), startup funds from the City University of Hong Kong (9380154), TBSC Project fund and Futian research project (9609327).

References

1. Schlieper G, Kruger T, Djuric Z, Damjanovic T, Markovic N, Schurgers LJ, et al. Vascular access calcification predicts mortality in hemodialysis patients. *Kidney Int.* 2008;74(12):1582-7.
2. Zhang W, Sun Y, Yang Y, and Chen Y. Impaired intracellular calcium homeostasis enhances protein O-GlcNAcylation and promotes vascular calcification and stiffness in diabetes. *Redox Biol.* 2023;63:102720.
3. Timmis A, Townsend N, Gale C, Grobbee R, Maniadakis N, Flather M, et al. European Society of Cardiology: Cardiovascular Disease Statistics 2017. *Eur Heart J.* 2018;39(7):508-79.
4. Lanzer P, Boehm M, Sorribas V, Thiriet M, Janzen J, Zeller T, et al. Medial vascular calcification revisited: review and perspectives. *Eur Heart J.* 2014;35(23):1515-25.
5. Shanahan CM. Mechanisms of vascular calcification in CKD-evidence for premature ageing? *Nat Rev Nephrol.* 2013;9(11):661-70.
6. Ouyang L, Su X, Li W, Tang L, Zhang M, Zhu Y, et al. ALKBH1-demethylated DNA N6-methyladenine modification triggers vascular calcification via osteogenic reprogramming in chronic kidney disease. *J Clin Invest.* 2021;131(14).
7. Li W, Feng W, Su X, Luo D, Li Z, Zhou Y, et al. SIRT6 protects vascular smooth muscle cells from osteogenic transdifferentiation via Runx2 in chronic kidney disease. *J Clin Invest.* 2022;132(1).
8. Furmanik M, Chatrou M, van Gorp R, Akbulut A, Willems B, Schmidt H, et al. Reactive Oxygen-Forming Nox5 Links Vascular Smooth Muscle Cell Phenotypic Switching and Extracellular Vesicle-Mediated Vascular Calcification. *Circ Res.* 2020;127(7):911-27.
9. Alexander MR, and Owens GK. Epigenetic control of smooth muscle cell differentiation and phenotypic switching in vascular development and disease. *Annu Rev Physiol.* 2012;74:13-40.
10. Lacolley P, Regnault V, Segers P, and Laurent S. Vascular Smooth Muscle Cells and Arterial Stiffening: Relevance in Development, Aging, and Disease. *Physiol Rev.* 2017;97(4):1555-617.
11. Petsophonsakul P, Burgmaier M, Willems B, Heeneman S, Stadler N, Gremse F, et al. Nicotine promotes vascular calcification via intracellular Ca2+-mediated, Nox5-induced oxidative stress, and extracellular vesicle release in vascular smooth muscle cells. *Cardiovasc Res.* 2022;118(9):2196-210.
12. Chen Y, Zhao X, and Wu H. Arterial Stiffness: A Focus on Vascular Calcification and Its Link to Bone Mineralization. *Arterioscler Thromb Vasc Biol.* 2020;40(5):1078-93.
13. Chen Y, Zhao X, and Wu H. Transcriptional Programming in Arteriosclerotic Disease: A Multifaceted Function of the Runx2 (Runt-Related Transcription Factor 2). *Arterioscler Thromb Vasc Biol.* 2021;41(1):20-34.
14. Byon CH, Javed A, Dai Q, Kappes JC, Clemens TL, Darley-Usmar VM, et al. Oxidative stress induces vascular calcification through modulation of the osteogenic transcription factor Runx2 by AKT signaling. *J Biol Chem.* 2008;283(22):15319-27.
15. Shao JS, Cai J, and Towler DA. Molecular mechanisms of vascular calcification: lessons learned from the aorta. *Arterioscler Thromb Vasc Biol.* 2006;26(7):1423-30.
16. Steitz SA, Speer MY, Curinga G, Yang HY, Haynes P, Aebersold R, et al. Smooth muscle

cell phenotypic transition associated with calcification: upregulation of Cbfa1 and downregulation of smooth muscle lineage markers. *Circ Res.* 2001;89(12):1147-54.

17. Engelse MA, Neele JM, Bronckers AL, Pannekoek H, and de Vries CJ. Vascular calcification: expression patterns of the osteoblast-specific gene core binding factor alpha-1 and the protective factor matrix gla protein in human atherogenesis. *Cardiovasc Res.* 2001;52(2):281-9.
18. Tyson KL, Reynolds JL, McNair R, Zhang Q, Weissberg PL, and Shanahan CM. Osteo/chondrocytic transcription factors and their target genes exhibit distinct patterns of expression in human arterial calcification. *Arterioscler Thromb Vasc Biol.* 2003;23(3):489-94.
19. Sun Y, Byon CH, Yuan K, Chen J, Mao X, Heath JM, et al. Smooth muscle cell-specific runx2 deficiency inhibits vascular calcification. *Circ Res.* 2012;111(5):543-52.
20. Heath JM, Sun Y, Yuan K, Bradley WE, Litovsky S, Dell'Italia LJ, et al. Activation of AKT by O-linked N-acetylglucosamine induces vascular calcification in diabetes mellitus. *Circ Res.* 2014;114(7):1094-102.
21. Lin ME, Chen T, Leaf EM, Speer MY, and Giachelli CM. Runx2 Expression in Smooth Muscle Cells Is Required for Arterial Medial Calcification in Mice. *Am J Pathol.* 2015;185(7):1958-69.
22. Ito S, D'Alessio AC, Taranova OV, Hong K, Sowers LC, and Zhang Y. Role of Tet proteins in 5mC to 5hmC conversion, ES-cell self-renewal and inner cell mass specification. *Nature.* 2010;466(7310):1129-33.
23. Potus F, Pauciulo MW, Cook EK, Zhu N, Hsieh A, Welch CL, et al. Novel Mutations and Decreased Expression of the Epigenetic Regulator TET2 in Pulmonary Arterial Hypertension. *Circulation.* 2020;141(24):1986-2000.
24. Soubrier F. TET2: A Bridge Between DNA Methylation and Vascular Inflammation. *Circulation.* 2020;141(24):2001-3.
25. Gumuser ED, Schuermans A, Cho SMJ, Sporn ZA, Uddin MM, Paruchuri K, et al. Clonal Hematopoiesis of Indeterminate Potential Predicts Adverse Outcomes in Patients With Atherosclerotic Cardiovascular Disease. *J Am Coll Cardiol.* 2023;81(20):1996-2009.
26. Kuhnert S, Mansouri S, Rieger MA, Savai R, Avci E, Diaz-Pina G, et al. Association of Clonal Hematopoiesis of Indeterminate Potential with Inflammatory Gene Expression in Patients with COPD. *Cells.* 2022;11(13).
27. Abplanalp WT, Mas-Peiro S, Cremer S, John D, Dimmeler S, and Zeiher AM. Association of Clonal Hematopoiesis of Indeterminate Potential With Inflammatory Gene Expression in Patients With Severe Degenerative Aortic Valve Stenosis or Chronic Postischemic Heart Failure. *JAMA Cardiol.* 2020;5(10):1170-5.
28. Liu R, Jin Y, Tang WH, Qin L, Zhang X, Tellides G, et al. Ten-eleven translocation-2 (TET2) is a master regulator of smooth muscle cell plasticity. *Circulation.* 2013;128(18):2047-57.
29. Drissi H, Luc Q, Shakoori R, Chuva De Sousa Lopes S, Choi JY, Terry A, et al. Transcriptional autoregulation of the bone related CBFA1/RUNX2 gene. *J Cell Physiol.* 2000;184(3):341-50.
30. Harada H, Tagashira S, Fujiwara M, Ogawa S, Katsumata T, Yamaguchi A, et al. Cbfa1 isoforms exert functional differences in osteoblast differentiation. *J Biol Chem.* 1999;274(11):6972-8.

31. Zeng Q, Song J, Sun X, Wang D, Liao X, Ding Y, et al. A negative feedback loop between TET2 and leptin in adipocyte regulates body weight. *Nat Commun.* 2024;15(1):2825.
32. Huerga Encabo H, Aramburu IV, Garcia-Albornoz M, Piganeau M, Wood H, Song A, et al. Loss of TET2 in human hematopoietic stem cells alters the development and function of neutrophils. *Cell Stem Cell.* 2023;30(6):781-99 e9.
33. Williams K, Christensen J, Pedersen MT, Johansen JV, Cloos PA, Rappsilber J, et al. TET1 and hydroxymethylcytosine in transcription and DNA methylation fidelity. *Nature.* 2011;473(7347):343-8.
34. Chen Q, Chen Y, Bian C, Fujiki R, and Yu X. TET2 promotes histone O-GlcNAcylation during gene transcription. *Nature.* 2013;493(7433):561-4.
35. Deplus R, Delatte B, Schwinn MK, Defrance M, Mendez J, Murphy N, et al. TET2 and TET3 regulate GlcNAcylation and H3K4 methylation through OGT and SET1/COMPASS. *EMBO J.* 2013;32(5):645-55.
36. Zhang Q, Zhao K, Shen Q, Han Y, Gu Y, Li X, et al. Tet2 is required to resolve inflammation by recruiting Hdac2 to specifically repress IL-6. *Nature.* 2015;525(7569):389-93.
37. Iyer LM, Tahiliani M, Rao A, and Aravind L. Prediction of novel families of enzymes involved in oxidative and other complex modifications of bases in nucleic acids. *Cell Cycle.* 2009;8(11):1698-710.
38. Ko M, An J, Bandukwala HS, Chavez L, Aijo T, Pastor WA, et al. Modulation of TET2 expression and 5-methylcytosine oxidation by the CXXC domain protein IDAX. *Nature.* 2013;497(7447):122-6.
39. Ko M, Huang Y, Jankowska AM, Pape UJ, Tahiliani M, Bandukwala HS, et al. Impaired hydroxylation of 5-methylcytosine in myeloid cancers with mutant TET2. *Nature.* 2010;468(7325):839-43.
40. Tahiliani M, Koh KP, Shen Y, Pastor WA, Bandukwala H, Brudno Y, et al. Conversion of 5-methylcytosine to 5-hydroxymethylcytosine in mammalian DNA by MLL partner TET1. *Science.* 2009;324(5929):930-5.
41. Kim RH, Wang D, Tsang M, Martin J, Huff C, de Caestecker MP, et al. A novel smad nuclear interacting protein, SNIP1, suppresses p300-dependent TGF-beta signal transduction. *Genes Dev.* 2000;14(13):1605-16.
42. Chen LL, Lin HP, Zhou WJ, He CX, Zhang ZY, Cheng ZL, et al. SNIP1 Recruits TET2 to Regulate c-MYC Target Genes and Cellular DNA Damage Response. *Cell Rep.* 2018;25(6):1485-500 e4.
43. Chng Z, Teo A, Pedersen RA, and Vallier L. SIP1 mediates cell-fate decisions between neuroectoderm and mesendoderm in human pluripotent stem cells. *Cell Stem Cell.* 2010;6(1):59-70.
44. Wu M, Wu S, Chen W, and Li YP. The roles and regulatory mechanisms of TGF-beta and BMP signaling in bone and cartilage development, homeostasis and disease. *Cell Res.* 2024;34(2):101-23.
45. Salazar VS, Gamer LW, and Rosen V. BMP signalling in skeletal development, disease and repair. *Nat Rev Endocrinol.* 2016;12(4):203-21.
46. Watson KE, Bostrom K, Ravindranath R, Lam T, Norton B, and Demer LL. TGF-beta 1 and 25-hydroxycholesterol stimulate osteoblast-like vascular cells to calcify. *J Clin Invest.* 1994;93(5):2106-13.

47. Cui H, Yi H, Bao H, Tan Y, Tian C, Shi X, et al. The SWI/SNF chromatin remodeling factor DPF3 regulates metastasis of ccRCC by modulating TGF-beta signaling. *Nat Commun.* 2022;13(1):4680.
48. Ostriker AC, Xie Y, Chakraborty R, Sizer AJ, Bai Y, Ding M, et al. TET2 Protects Against Vascular Smooth Muscle Cell Apoptosis and Intimal Thickening in Transplant Vasculopathy. *Circulation.* 2021;144(6):455-70.
49. Owens GK, Kumar MS, and Wamhoff BR. Molecular regulation of vascular smooth muscle cell differentiation in development and disease. *Physiol Rev.* 2004;84(3):767-801.
50. Lee MH, Kim YJ, Yoon WJ, Kim JI, Kim BG, Hwang YS, et al. Dlx5 specifically regulates Runx2 type II expression by binding to homeodomain-response elements in the Runx2 distal promoter. *J Biol Chem.* 2005;280(42):35579-87.
51. Zambotti A, Makhluf H, Shen J, and Ducy P. Characterization of an osteoblast-specific enhancer element in the CBFA1 gene. *J Biol Chem.* 2002;277(44):41497-506.
52. Wu H, D'Alessio AC, Ito S, Xia K, Wang Z, Cui K, et al. Dual functions of Tet1 in transcriptional regulation in mouse embryonic stem cells. *Nature.* 2011;473(7347):389-93.
53. Guallar D, Bi X, Pardavila JA, Huang X, Saenz C, Shi X, et al. RNA-dependent chromatin targeting of TET2 for endogenous retrovirus control in pluripotent stem cells. *Nat Genet.* 2018;50(3):443-51.
54. Cobo I, Tanaka TN, Chandra Mangalhara K, Lana A, Yeang C, Han C, et al. DNA methyltransferase 3 alpha and TET methylcytosine dioxygenase 2 restrain mitochondrial DNA-mediated interferon signaling in macrophages. *Immunity.* 2022;55(8):1386-401 e10.
55. Ito K, Lee J, Chrysanthou S, Zhao Y, Josephs K, Sato H, et al. Non-catalytic Roles of Tet2 Are Essential to Regulate Hematopoietic Stem and Progenitor Cell Homeostasis. *Cell Rep.* 2019;28(10):2480-90 e4.
56. Smith E, and Shilatifard A. The chromatin signaling pathway: diverse mechanisms of recruitment of histone-modifying enzymes and varied biological outcomes. *Mol Cell.* 2010;40(5):689-701.
57. Zeng P, Yang J, Liu L, Yang X, Yao Z, Ma C, et al. ERK1/2 inhibition reduces vascular calcification by activating miR-126-3p-DKK1/LRP6 pathway. *Theranostics.* 2021;11(3):1129-46.

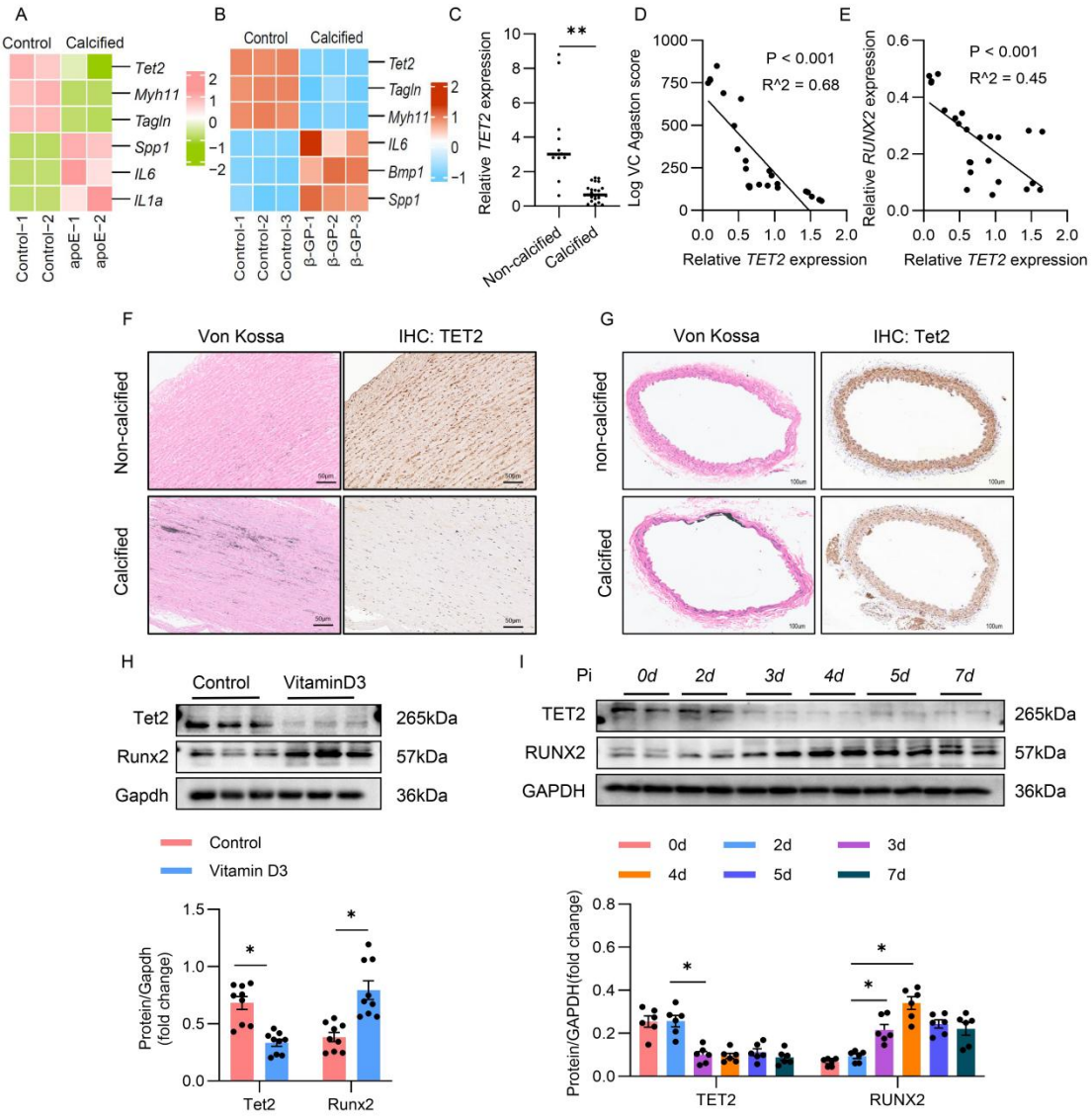

Figure 1: TET2 is negatively correlated with VC in both human and mice specimens. (A and B) Heatmap showed *TET2*, SMC markers (*Myh11, Tagln*), and osteogenic markers (*Spp1,IL6,IL1a, Bmp1*) mRNA expression in the control and the *apoE-/-* calcified mice aorta (A), and the β-GP treatment induced calcified mice aorta (B). (C) Leukocyte *TET2* mRNA expression in CKD patients with (VC, n = 21) or without (non-VC, n = 12) vascular calcification. (D) Correlation between Leukocyte *TET2* mRNA expression and calcific score (D), or RUNX2 mRNA expression (E) in CKD patients with calcification (VC, n = 21). (F) Von Kcossa staining and Immunohistochemical images of TET2 expression in the control and calcified arteries from patients with CKD. Scale bars: 50μm. n = 6. (G) Von Kcossa staining and Immunohistochemical images of Tet2 expression in the control and calcified mice arteries, Scale bars: 100μm, n = 3. (H and I) Western blot analysis and quantification of TET2 and RUNX2 expressions in calcified mice arteries and control groups (H) (n = 3), or in hVSMC induced by Pi for the indicated time (I), (n = 3). All values are presented as mean ± SEM. *P<0.05, **P<0.01. Statistical significance was assessed using 2-tailed t tests (C), one-way ANOVA followed by Dunnett’s test (H and I), and Pearson’s correlation coefficient analysis (D and E).

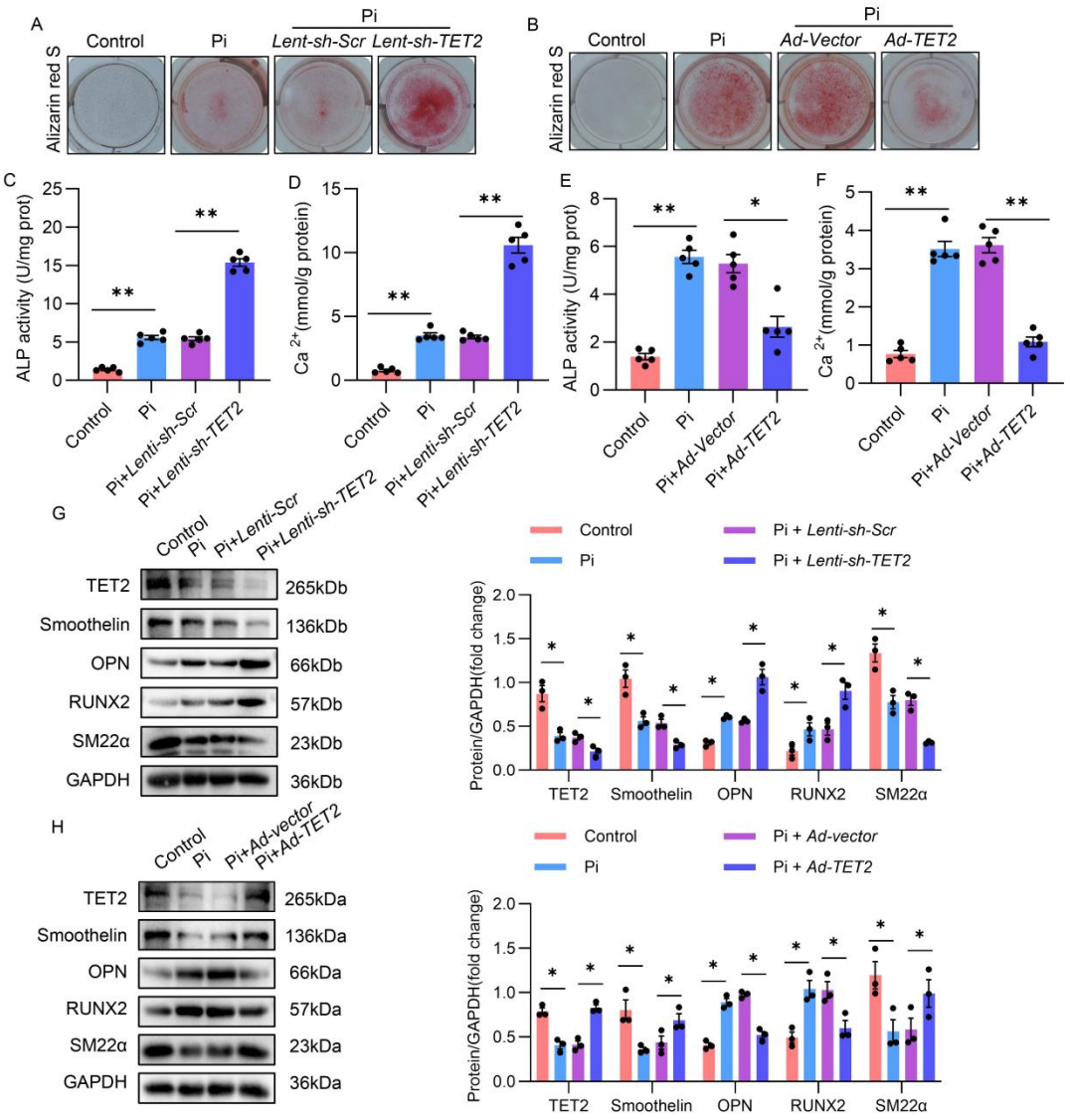

856

Figure 2: TET2 plays a role in human primary VSMC osteogenic transdifferentiation. (A and B) Alizarin red staining of hVSMC transfected with *Lenti-sh-Scr* or with *Lenti-sh-TET2* (A), and transfected with *Ad-Vector* or *Ad-TET2* (B) (n = 3). (C and D) ALP activity assay (C), quantification of calcium content (D) in hVSMC transfected with *Lenti-sh-Scr* or *Lenti-sh-TET2* (n = 5). (E and F) ALP activity assay (E), quantification of calcium content (F) in hVSMC transfected with *Ad-Vector* or *Ad-TET2* (n = 5). (G and H) Western blot analysis and quantification of TET2, RUNX2, OPN, Smoothelin, SM22α expression in hVSMC transfected with *Lenti-sh-Scr* or with *Lenti-sh-TET2* (G), and transfected with *Ad-Vector* or *Ad-TET2* (H) (n = 3). All values are presented as mean ± SEM. *P<0.05, **P<0.01. Statistical significance was assessed using one-way ANOVA followed by Dunnett's test (C-H).

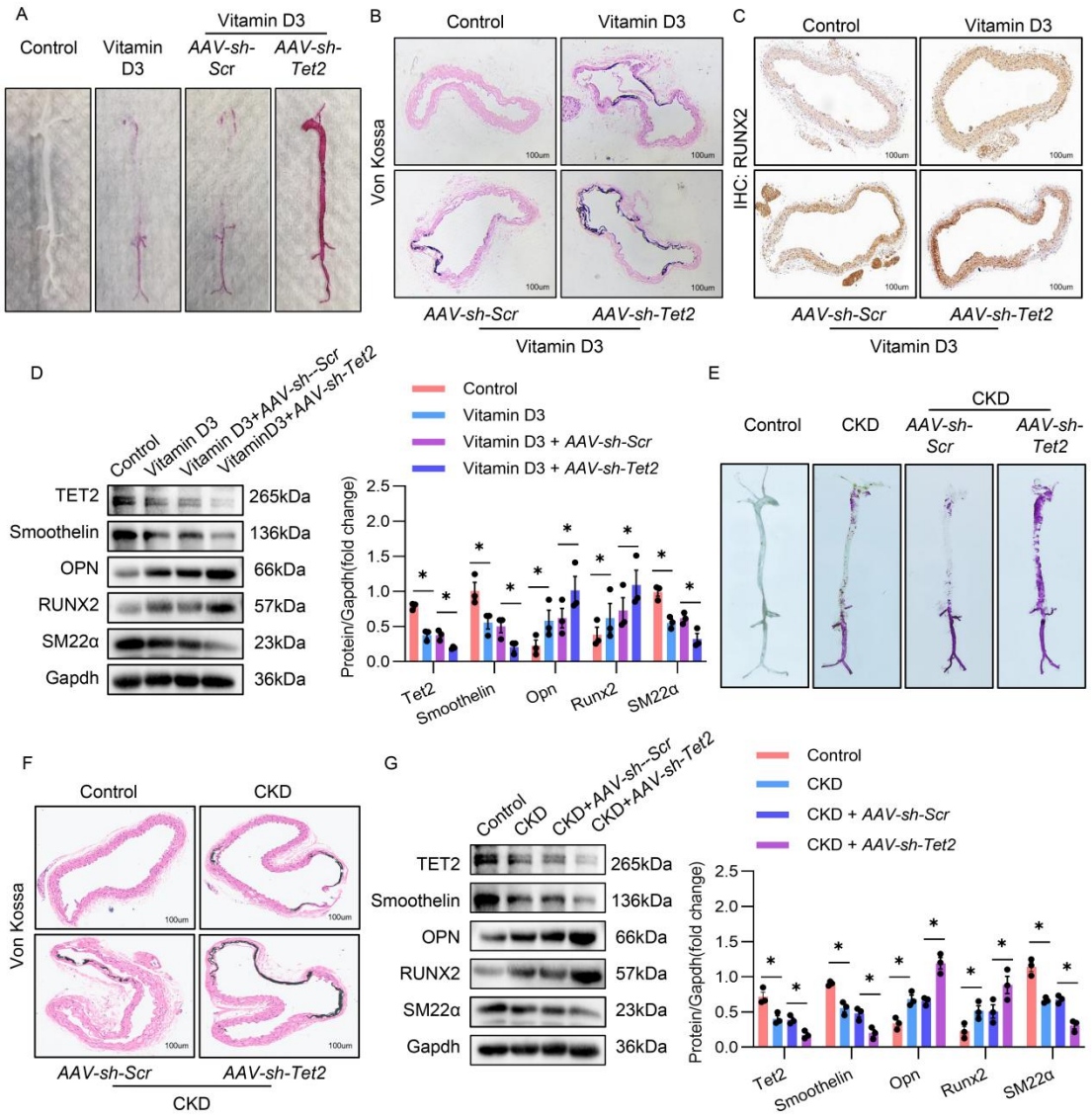

857

Figure 3: VSMC specific loss of Tet2 in mice aggravated vascular calcification. (A) Representative Alizarin Red S staining images of whole aortas from mice of control, injected with Vitamin D3, and Vitamin D3 together with *AAV-sh-Scr* or *AAV-sh-Tet2* (n = 3). (B) Representative Von Kossa staining of the aortic sections from the mice of control, injected with Vitamin D3, and Vitamin D3 together with *AAV-sh-Scr* or *AAV-sh-Tet2*, Scale bars: 100μm, (n = 3). (C) Representative Immunohistochemical images of Runx2 expression in the aortic sections from mice of control, injected with Vitamin D3, and Vitamin D3 together with *AAV-sh-Scr* or *AAV-sh-Tet2*, Scale bars: 100μm (n = 3). (D) Western blot analysis and quantification of Tet2 and osteogenic phenotypic markers (Runx2 and Opn) and contractile phenotype marker (Smoothelin and SM22α) expression in aortas from mice of control, injected with Vitamin D3, and Vitamin D3 together with *AAV-sh-Scr* or *AAV-sh-Tet2*, (n = 3). (E) Representative Alizarin Red S staining images of whole aortas from mice of control, CKD, and CKD injected with *AAV-sh-Scr* or *AAV-sh-Tet2* (n = 3). (F) Representative Von Kossa staining of the aortic sections from the mice of control, CKD, and CKD injected with *AAV-sh-Scr* or *AAV-sh-Tet2*, Scale bars: 100μm, (n = 3). (G) Western blot analysis and quantification of Tet2 and osteogenic phenotypic markers (Runx2 and Opn) and contractile phenotype marker (Smoothelin and SM22α) expression in aortas from mice of control, CKD, and CKD injected with *AAV-sh-Scr* or *AAV-sh-Tet2*, (n = 3). All values are presented as mean ± SEM. *P<0.05, **P<0.01. Statistical significance was assessed using one-way ANOVA followed by Dunnett's test (D and G).

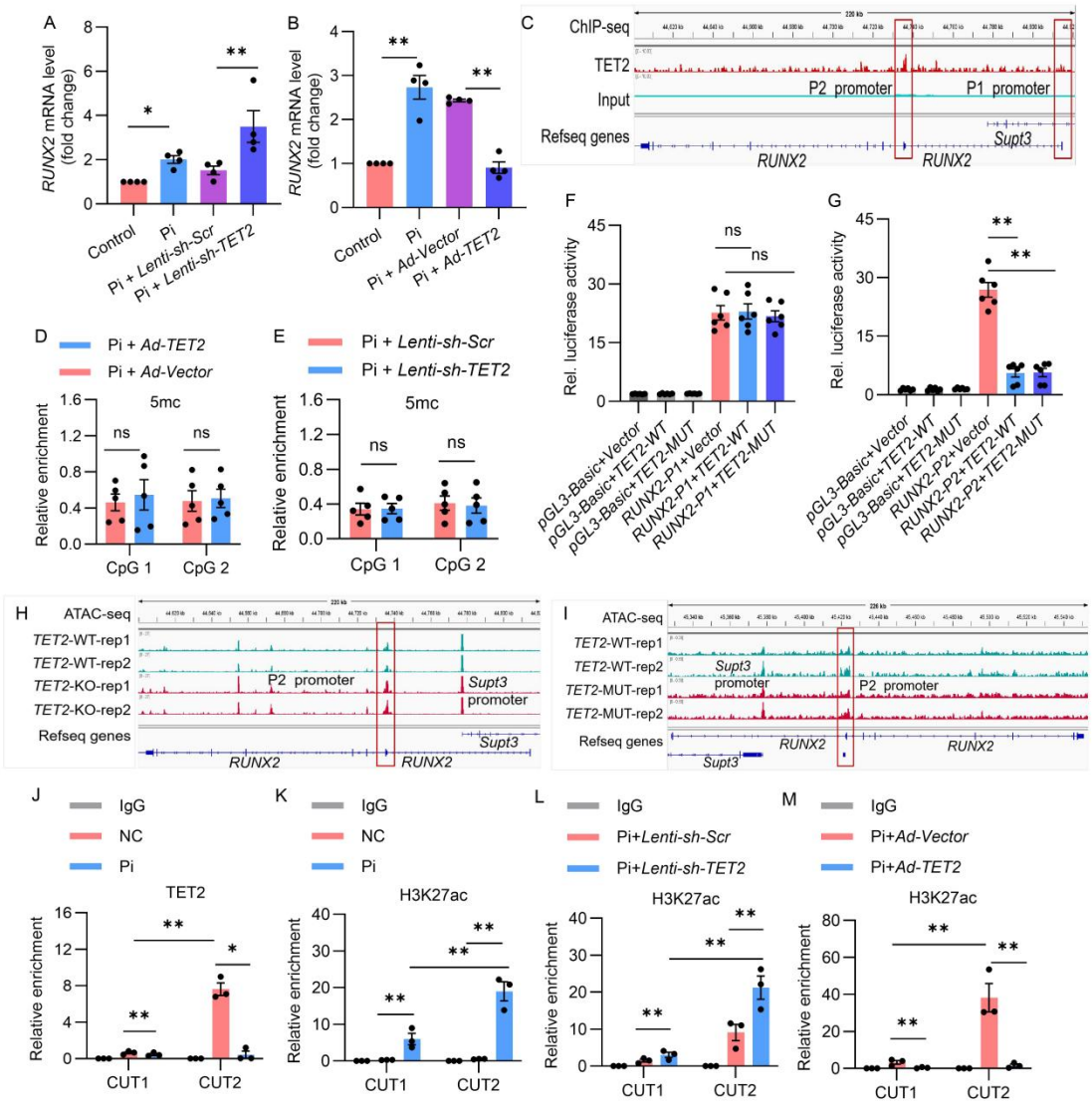

858

Figure 4: TET2 inhibits *RUNX2* gene transcription not by DNA demethylation but by decreasing H3K27ac on the P2 promoter. (A and B) Quantitative real-time PCR analysis of *RUNX2* expression in hVSMCs transfected with *Lenti-sh-Scr* or *Lenti-sh-TET2*(A), or *Ad-Vector* or *Ad-TET2* (B) (n = 4). (C) CHIP-seq analysis for TET2 enrichments on *RUNX2* gene. (D and E) DNA methylation quantified by MethylCap-qPCR in *RUNX2* P2 promoter from hVSMCs with TET2 overexpression (D) or TET2 knockdown (E), (n = 5). (F and G) Luciferase activity analyzed after co-transfection with control Renilla luciferase plasmid and constructs of *RUNX2* P1 promoter (F) or P2 promoter-driven luciferase reporters (G), and co-transfection either with control, wild type *TET2* (*TET2*-WT) or enzyme activity loci mutate *TET2* (*TET2*-MUT) (n = 6). (H) ATAC-seq analysis for *RUNX2* gene transposase accessible chromatin in *TET2*-WT and *TET2*-KO groups. (I) ATAC-seq analysis for *RUNX2* gene transposase accessible chromatin in *TET2*-WT and *TET2*-MUT groups. (J and K) TET2 CUT&Tag-qPCR (J) and H3K27ac CUT&Tag-qPCR (K) at *RUNX2* (CUT1) P1 and (CUT2) P2 promoter in hVSMC with either a control or exposed to Pi (n=3). (L and M) H3K27ac CUT&Tag-qPCR at *RUNX2* (CUT1) P1 and (CUT2) P2 promoter in hVSMC with either a TET2 knockdown (L) or TET2 overexpression (M) (n = 3). All values are presented as mean ± SD *P<0.05, **P<0.01. Statistical significance was assessed using one-way ANOVA followed by Dunnett's test (A,B,D-G and J-M).

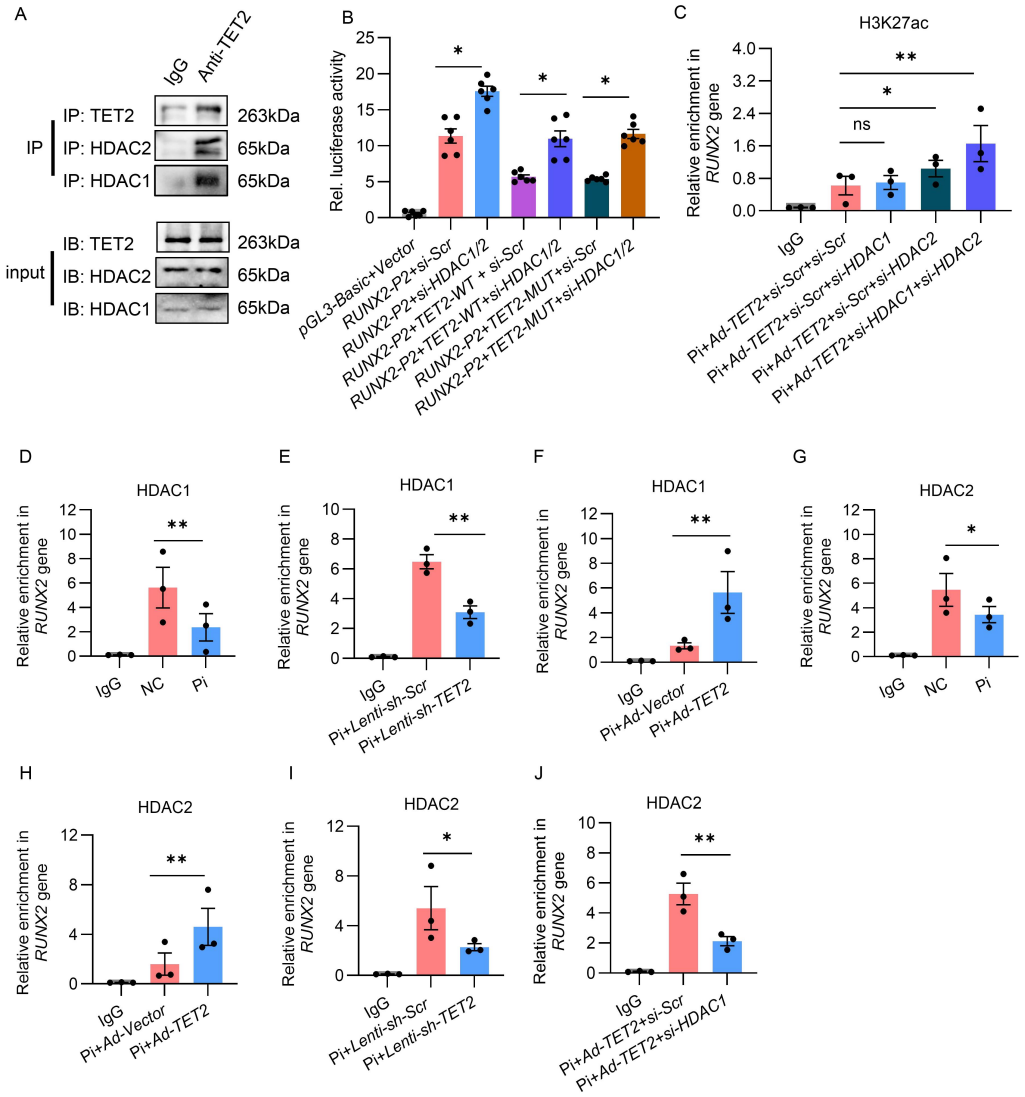

859

Figure 5: TET2 interact with HDAC1/2 to suppress the activity of *RUNX2* P2 promoter through deacetylating H3K27ac. (A) Co-immunoprecipitation (IP) analysis to detect the interaction between TET2 and HDAC1/2 in hVSMC. (B) pretreatment with control or HDAC1/2 knockdown, luciferase activities were analyzed after co-transfection with control Renilla luciferase plasmid and constructs of *RUNX2* P2 promoter-driven luciferase reporters, and co-transfection either with control, wild type *TET2* or enzyme activity loci mutate *TET2* (n = 6 per group). (C) H3K27ac CUT&Tag-qPCR at RUNX2 P2 promoter in hVSMCs transfected *si-Scr*, *si-HDAC1*, *HDAC2* or *HDAC1/2*, together with TET2 overexpression (n = 3 per group). (D-I) HDAC1 CUT&Tag-qPCR (D-F) or HDAC2 CUT&Tag-qPCR (G-I) at *RUNX2* P2 promoter in hVSMC with either Pi (D and G), TET2 knockdown (E and I), or TET2 overexpression (F and H) (n = 3 per group). (J) HDAC2 CUT&Tag-qPCR at *RUNX2* P2 promoter in TET2 overexpressed hVSMCs with either a control or HDAC1 knockdown, (n = 3 per group). All values are presented as mean ± SEM, *P<0.05, **P<0.01. Statistical significance was assessed using one-way ANOVA followed by Dunnett's test (B-J).

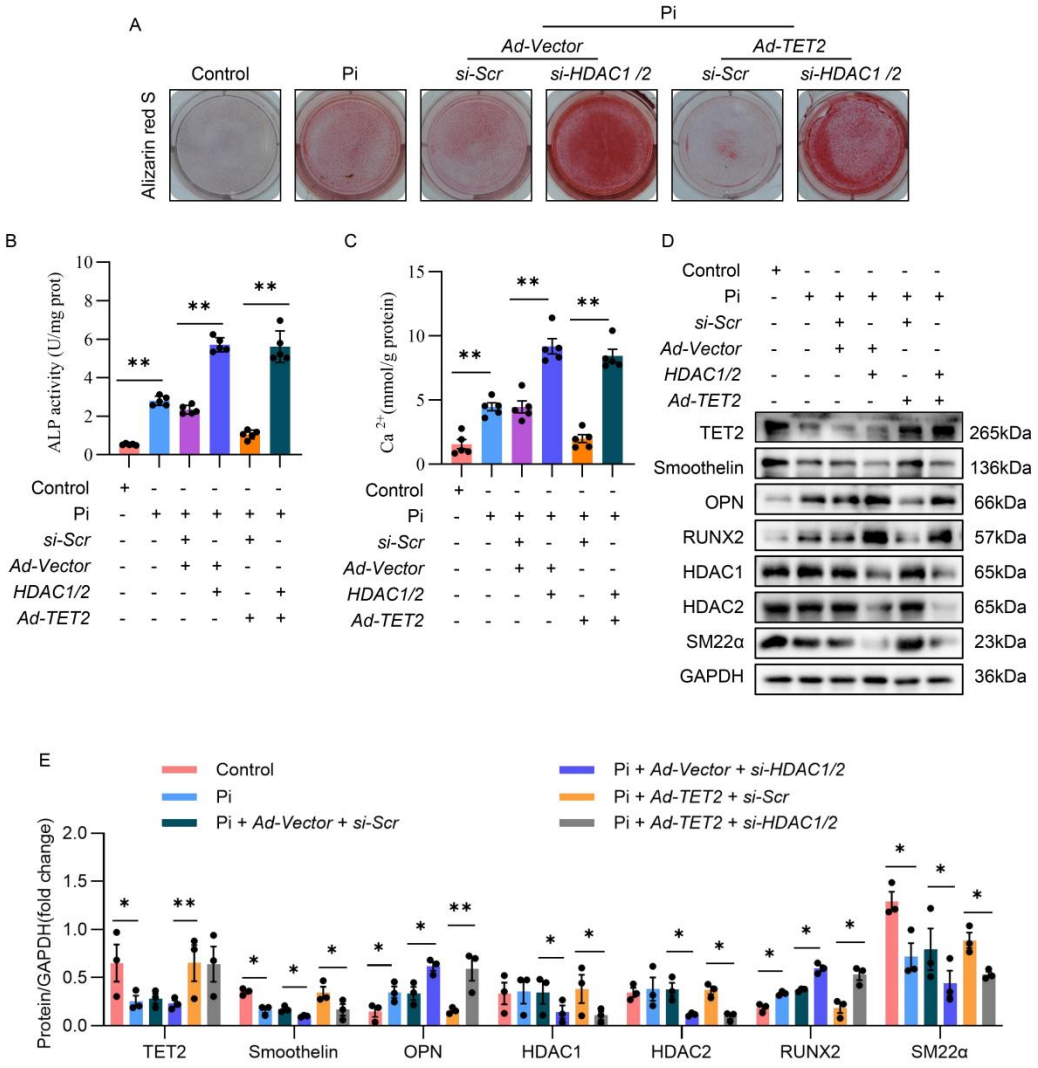

860

Figure 6: TET2 inhibits hVSMCs osteogenic transdifferentiation by interacting with HDAC1/2. (A) Alizarin red staining of in hVSMCs transfected *si-Scr* or *si-HDAC1/2* together with *Ad-Vector* or *Ad-TET2* (n = 3 per group). (B and C) ALP activity assay (B), quantification of calcium content (C) in hVSMCs transfected *si-Scr* or *si-HDAC1/2* together with *Ad-Vector* or *Ad-TET2* (n = 5 per group). (D and E) Western blot analysis and quantification of TET2, RUNX2, OPN, Smoothelin, SM22, HDAC1/2 expression in hVSMCs transfected *si-Scr* or *si-HDAC1/2* together with *Ad-Vector* or *Ad-TET2* (n = 3 per group). All values are presented as mean ± SEM, *P<0.05, **P<0.01. Statistical significance was assessed using one-way ANOVA followed by Dunnett's test (B, C and E).

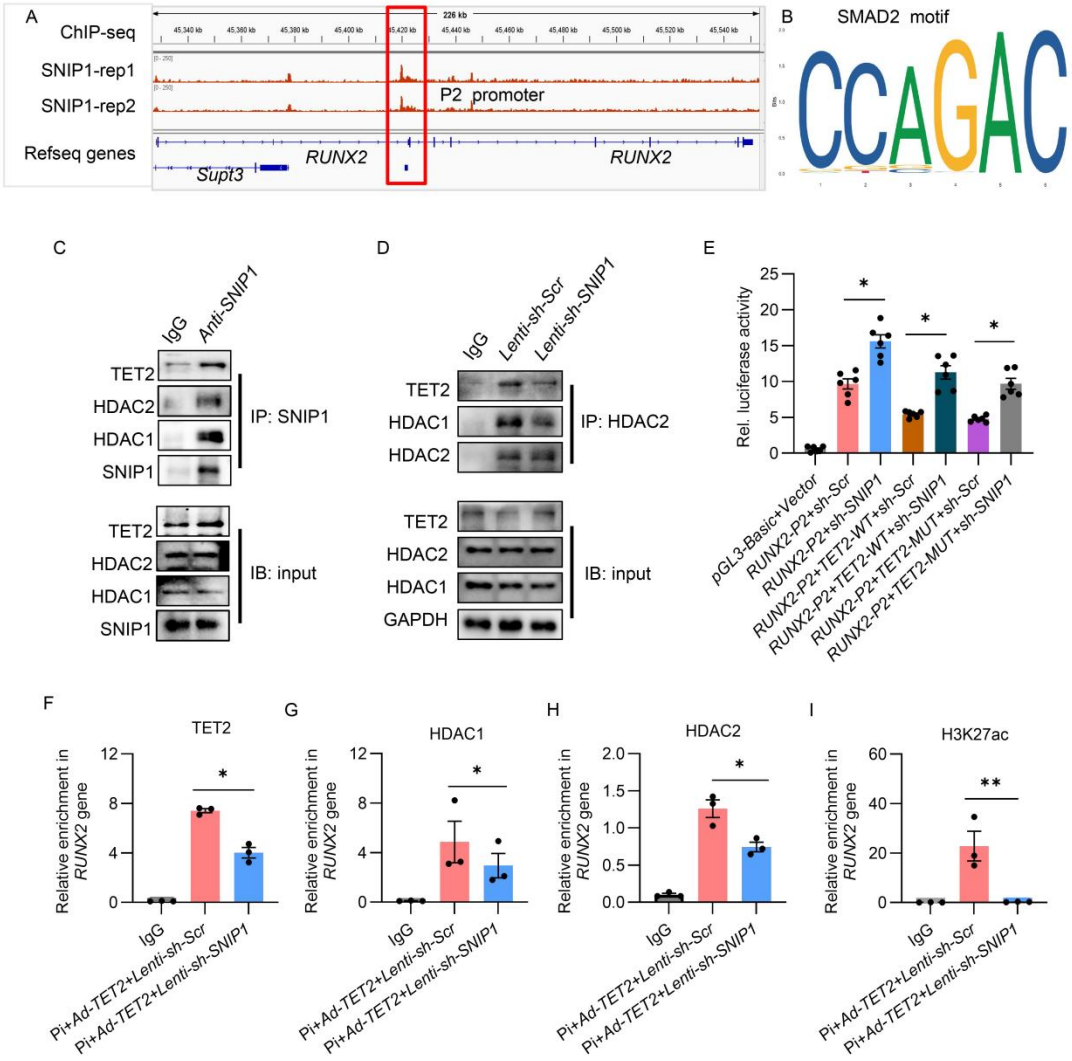

861

Figure 7: SNIP1 is necessary for TET2 to interact with HDAC1/2 at the *RUNX2* P2 promoter. (A) ChIP-seq analysis for SNIP1 enrichments on *RUNX2* gene. (B) SMAD2 binding motif. (C) Co-immunoprecipitation (Co-IP) to detect the interaction between SNIP1, TET2 and HDAC1/2 in hVSMCs. (D) VSMC pre-transfected with *Lenti-sh-Scr* or *Lenti-sh-SNIP1*, Co-immunoprecipitation (IP) analysis to detect the interaction between TET2 and HDAC1/2 in hVSMCs. (E) Cells pre-infected with *Lenti-sh-Scr* or *Lenti-sh-SNIP1*, luciferase activity analyzed after co-transfection with control Renilla luciferase plasmid and constructs of the P2 promoter-driven luciferase reporters, and co-transfection either with control, wild type *TET2* or enzyme activity loci mutate *TET2*, (n = 6 per group). (F-I) TET2 CUT&Tag-qPCR (F), HDAC1 CUT&Tag-qPCR (G), HDAC2 CUT&Tag-qPCR (H), and H3K27ac CUT&Tag-qPCR (I) at the *RUNX2* P2 promoter in hVSMCs transfected with *Lenti-sh-Scr* or *Lenti-sh-SNIP1* together with TET2 overexpression, (n = 3 per group). All values are presented as mean ± SEM, *P<0.05, **P<0.01. Statistical significance was assessed using one-way ANOVA followed by Dunnett's test (E-I).

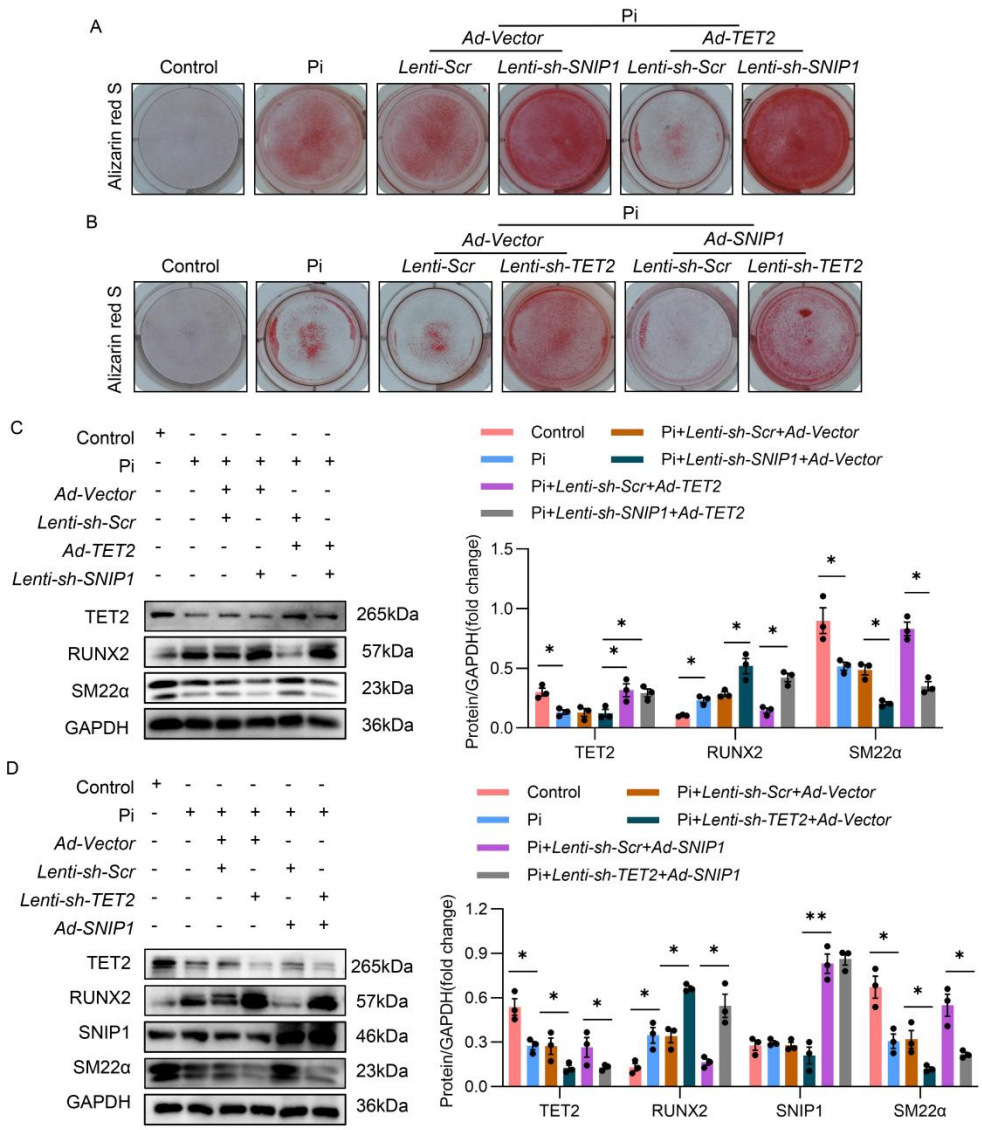

Figure 8: SNIP1 is vital for TET2 to hinder hVSMCs osteogenic transdifferentiation. (A and C) Alizarin red staining(A) and Western blot analysis and quantification(C) of hVSMCs transfected with *Lenti-sh-Scr* or *Lenti-sh-SNIP1* together with *TET2* overexpression or control vector (n=3 per group). (B and D) Alizarin red staining (B) and Western blot analysis and quantification (D) of hVSMCs transfected with *Lenti-sh-Scr* or *Lenti-sh-TET2* together with *SNIP1* overexpression or control vector (n = 3 per group). All values are presented as mean ± SEM, *P<0.05, **P<0.01. Statistical significance was assessed using one-way ANOVA followed by Dunnett's test (C and D).

873

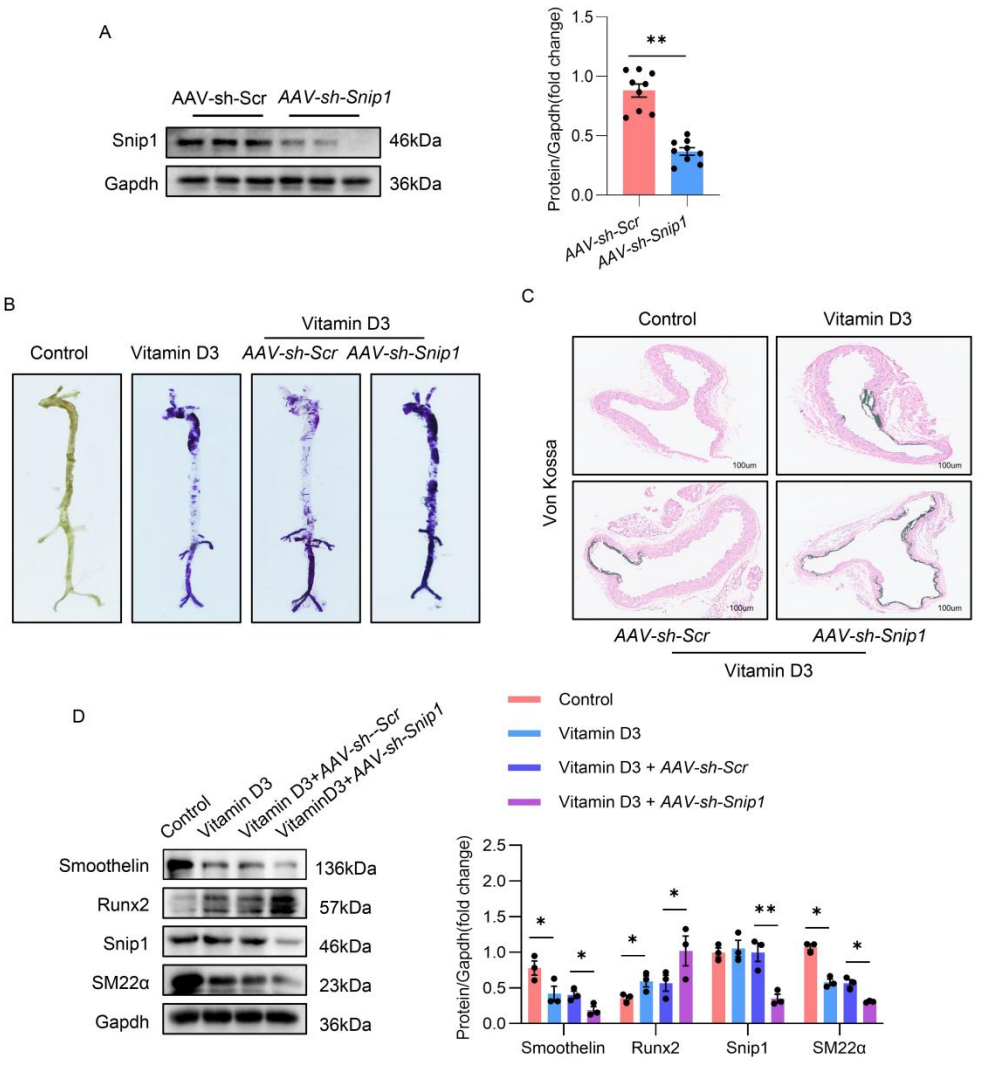

874

Figure 9: Knockdown of Snip1 accelerated vascular calcification in mice. (A) Western blot analysis and quantification of Snip1 expression in the aortas from mice injected with *AAV-sh-Scr* and *AAV-sh-Snip1* (n = 3 per group). (B) Representative Alizarin Red S staining images of the whole aortas from mice of control, injected with Vitamin D3, *AAV-sh-Scr*, and *AAV-sh-Snip1* (n = 3 per group). (C) Representative Von Kossa staining of the aortic sections from the mice of control, injected with Vitamin D3, *AAV-sh-Scr*, and *AAV-sh-Snip1*, Scale bars: 100μm, (n = 3 per group). (D) Western blot analysis and quantification of Snip1 and osteogenic phenotypic markers Runx2 and contractile phenotype markers (Smoothelin and SM22α) expression in the aortas from mice of control, injected with Vitamin D3, *AAV-sh-Scr*, and *AAV-sh-Snip1* (n = 3 per group). All values are presented as mean ± SEM. *P<0.05, **P<0.01. Statistical significance was assessed using Statistical significance was assessed using 2-tailed t tests (A), one-way ANOVA followed by Dunnett's test (D).